9A.3   SMOKE PLUME OPTICAL PROPERTIES AND TRANSPORT OBSERVED BY A MULTI-WAVELENGTH LIDAR, SUNPHOTOMETER AND SATELLITE

Lina Cordero*, Yonghua Wu, Barry Gross, Fred Moshary, Sam Ahmed
Optical Remote Sensing Lab, City College of New York, New York, NY, 10031

1. ABSTRACT

Forest-fire and biomass burning often inject large amounts of smoke aerosols into the atmosphere, which play important roles in climate radiation and air quality. In this study, the combined observations of smoke plumes from a ground-based multi-wavelength lidar, sun/sky radiometer and MODIS and CALIOP satellites are presented. We focus in particular on one representative event (the Idaho-Montana forest fire on August 14-15, 2007) to retrieve aerosol plumes optical characteristics and track their intra-continent transport. Multi-wavelength extinction profiles of aerosol plumes are first derived by constraining lidar profiles with sunphotometer-measured column aerosol optical depth (AOD), and then Angstrom exponents are obtained to discriminate smoke plumes from cloud and dust particles. Long-distance transport and origins of smoke plumes are illustrated by satellite MODIS/Aqua, Calipso/CALIOP imageries and NOAA/HYSPLIT air backward trajectory analysis. Importantly, we show that aloft smoke plumes may mix downward into the planetary boundary layer (PBL) and potentially result in the increase of surface $PM_{2.5}$ concentrations and that these mixings are a major factor in pollution enhancement during the summer when the PBL is more convective allowing for enhanced mixing.

2. INTRODUCTION

Smoke plume aerosols from forest fires can be elevated to the free troposphere and transported over long distances, thus affecting the environment and climate in the local and regional scale. For example, observations indicate that aerosol plumes potentially modify cloud physical, chemical and optical properties (Kaufman 2005; Sassen 2003, 2008). The occurrence, transport and column optical properties of smoke plumes have been extensively investigated by satellite-borne and ground-based radiometers (Kaufman et al., 1998; Torres et al., 2002; Hoff et al., 2005; Kahn et al., 2007), but the vertical structure of aerosol plumes are highly variables.

* *Corresponding author address:* Lina Cordero, The City College of New York, Dept. of Electrical Engineering, New York, NY 10031; e-mail: lcorder01@ccny.cuny.edu.

3. INSTRUMENTS AND METHODS

A ground-based multi-wavelength elastic-Raman scattering lidar has been operating in New York City (NYC, 40.821°N/73.949°W) (Wu 2009) since March 2006. A Nd:YAG laser (Spectra-physics Quanta-Ray 320) emits at the fundamental, double and triple harmonics (1064-532-355-nm) with a repetition rate of 30 Hz. Three elastic-scattering and two Raman-scattering returns by nitrogen and water vapor molecules excited by 355-nm are collected. The receiver telescope has a diameter of 50.8 cm and a field of view of 1~2 mrad. A Perkin-Elmer Si-APD (avalanche photodiode) is used to detect 1064-nm signal while PMTs (Hamamatsu photomultiplier tube) are used for the 355~532 wavelengths. Narrow-band interference filters (0.3~1 nm) are deployed in front of the detectors to suppress the background skylight. The signals are acquired by a LICEL transient recorder (TR40-160, 12-bit 40-MHz). With a coaxial transmitter-receiver geometry, full return signals are detected starting at 0.5 km. The return profiles are recorded at 1-min time averaging with a 3.75-m range resolution. The multi-wavelength measurement provides some level of particle size information by quantifying the wavelength dependence of the scattering parameters (i.e. Angstrom exponent). We focus on the elastic-scattering signals for deriving aloft plume optical properties in the day time because the Raman-channel capability is limited by the weak signal-to-noise ratio (SNR).

In addition, an AERONET Cimel sun/sky radiometer (CE-318) and a ceilometer (Vaisala CL-31) are co-located at the lidar site. The AERONET sunphotometer obtains aerosol optical depth (AOD) at wavelengths 340~1020 nm by measuring the direct solar radiance (Holben 1989). Aerosol microphysics parameters (volume size distribution and refractive index) are inverted from sky radiance measurements in the almucantar mode, and this inversion accuracy depends on the criteria such as solar zenith angle, sky-radiance error and aerosol optical depth (Dubovik 2000). The fine- and coarse-mode AODs are derived from the spectral derivatives of the AOD spectrum (O'Neil 2003). Fine mode (sub-micron) particles are generally associated with smoke and pollution aerosols while coarse mode (super micron) particles indicate the presences of dust, marine aerosol and cloud particles (Eck 1999). The ceilometer has the single-lens design of transmitter-receiver providing the sufficient overlap as close as 5-m range and therefore profiling aerosol distribution down to the surface (Münkel 2004). In particular, the ceilometer

data is used by us to extend the CCNY-lidar data into the overlap zone (0-0.5 km) allowing for the accurate retrieval of lidar S-ratio since the full column AOD from lidar can be compared to the sunphotometer. Meanwhile, a standard surface air quality monitoring station is deployed for $PM_{2.5}$ mass concentration nearby the lidar site (~100 m away) by the New York State Department of Environment Conservation (NYDEC).

In general, to obtain aerosol extinction and backscatter coefficients from elastic lidar returns, a constant lidar ratio and a far-end boundary of aerosol are usually assigned in the inversions (Klett 1981; Fernald 1984). The far-end reference altitude is often chosen in the upper troposphere (6~12 km altitude) where the air is relatively free-aerosol during non-volcanic periods. As the lidar-ratio varies from 10 to 100 sr. depending on the aerosol size distribution and chemical species (Ackerman 1998), the large uncertainty of the solution could be caused from an arbitrary lidar–ratio. To reduce this uncertainty, we use the sunphotometer-measured aerosol optical depth (SP-AOD) to constrain the lidar ratio and aerosol extinction profile, which means that the initially selected value of lidar ratio can be iteratively adjusted over 10~100 sr. until the lidar-derived aerosol optical depth matches the SP-AOD (Pelon 2002; Landulfo 2003). Thus with this approach, the uncertainty of the lidar-ratio is mainly from the SP-AOD uncertainty, which is between 0.01-0.02 (Pelon 2002).

Finally, with the lidar-measured multi-wavelength aerosol extinction coefficient profiles, the Angstrom exponent profile can be estimated as follows:

$$\mathring{a} = -\frac{\log[\,\alpha(\lambda_1)/\alpha(\lambda_2)\,]}{\log(\lambda_1/\lambda_2)} \qquad (1)$$

Where, å is the Angstrom exponent and α is the aerosol extinction coefficient and the subscripts represent two different wavelengths. å is an intensive parameter which indicates aerosol size information. Generally, small particles such as smoke aerosols have large Angstrom exponent whereas large particles such as dust, sea salt and thin cloud have a small Angstrom exponent (Eck 1999; Sassano 1989). Thus, this parameter can be used to discriminate aerosol types within the plume.

4. OBSERVATION RESULTS:

4.1. Smoke plume vertical distribution and optical properties observed by lidar/sunphotometer

A heavy smoke intrusion event was observed by the CCNY-lidar on August 14-15, 2007. Figure 1(a) shows the time-height cross section of the range-corrected lidar backscatter returns at 1064-nm on Aug. 14, 2007. The colorbar indicates the returns intensities with the warm color (yellow and red) representing aerosol layer, blue for the clean air, and dark red for cloud. Lidar data illustrate one dense aerosol plume layer at 6~8 km altitude arriving at ~16:00 pm (local time, LT) along with some light aerosol layers before 16:00 LT. Then on Aug. 15, 2007 in Figure 1(b), two separate dense plume layers were located at 2~4 km and 4.5~6.5 km altitude, respectively. The lower layer subsequently mixed downward into the PBL at ~14:00 LT.

To quantitatively analyze this event, we first plot the vertical distribution of aerosol extinction coefficients and Angstrom exponents at 1064-532 nm on Aug. 14-15. In Figure 1(c) on Aug. 14, large Angstrom exponents (1.7~2.0) in the aerosol plume layer at 6.0-8.0 km indicate the plumes are fine mode dominated. The column averaged lidar-ratios were then obtained with values of 69±9 sr., 42±2 sr., and 63±1 sr. at 532-, 1064- and 355-nm, respectively, which are consistent with the existing calculations for smoke types of aerosol (Omar 2005; Cattrall 2005). On Aug. 15 in Figure 1(d), the upper layer of smoke at 4.0~6 km has the extinction peak value of 0.3 km^{-1} at 532-nm with Angstrom exponent close to 2.0. An aerosol multi-layer structure can be identified but the stability of the Angstrom exponent implies the homogenous particle size information.

Sunphotometer-measured aerosol column optical properties (level-1.5 after cloud screening) are given in Figure 2. Figure 2(a) shows the total, fine-mode, and coarse-mode AOD at 500-nm and Angstrom exponent at 440-870 nm on Aug. 14. The total AOD sharply increases from 0.2 to 0.6 at ~16:00 LT on Aug. 14, which corresponds well with the lidar-measured plume intrusion in time. In particular, we note changes in the Angstrom signature (rising from 1.5 to 1.8 by late afternoon on Aug. 14) indicating an increase of fine mode particulates. Clearly, a large fraction of AOD is from the fine-mode particles.

The aerosol single-scattering albedo (SSA) from SP-inversion data is 0.85 at wavelength 675-nm, highly suggestive of absorbing aerosols. With the characteristics of large Angstrom exponent, fine-mode and large absorption, we can definitively classify these plume layers as smoke particles (Eck 1999). On Aug. 15 in Figure 2(b), the column AODs remained at a high level with values of 0.6~0.8 at 500-nm, and the Angstrom coefficients remained consistently high, indicating the same type of transported particulates. These results are also in good quantitative agreement with the CCNY-lidar retrievals.
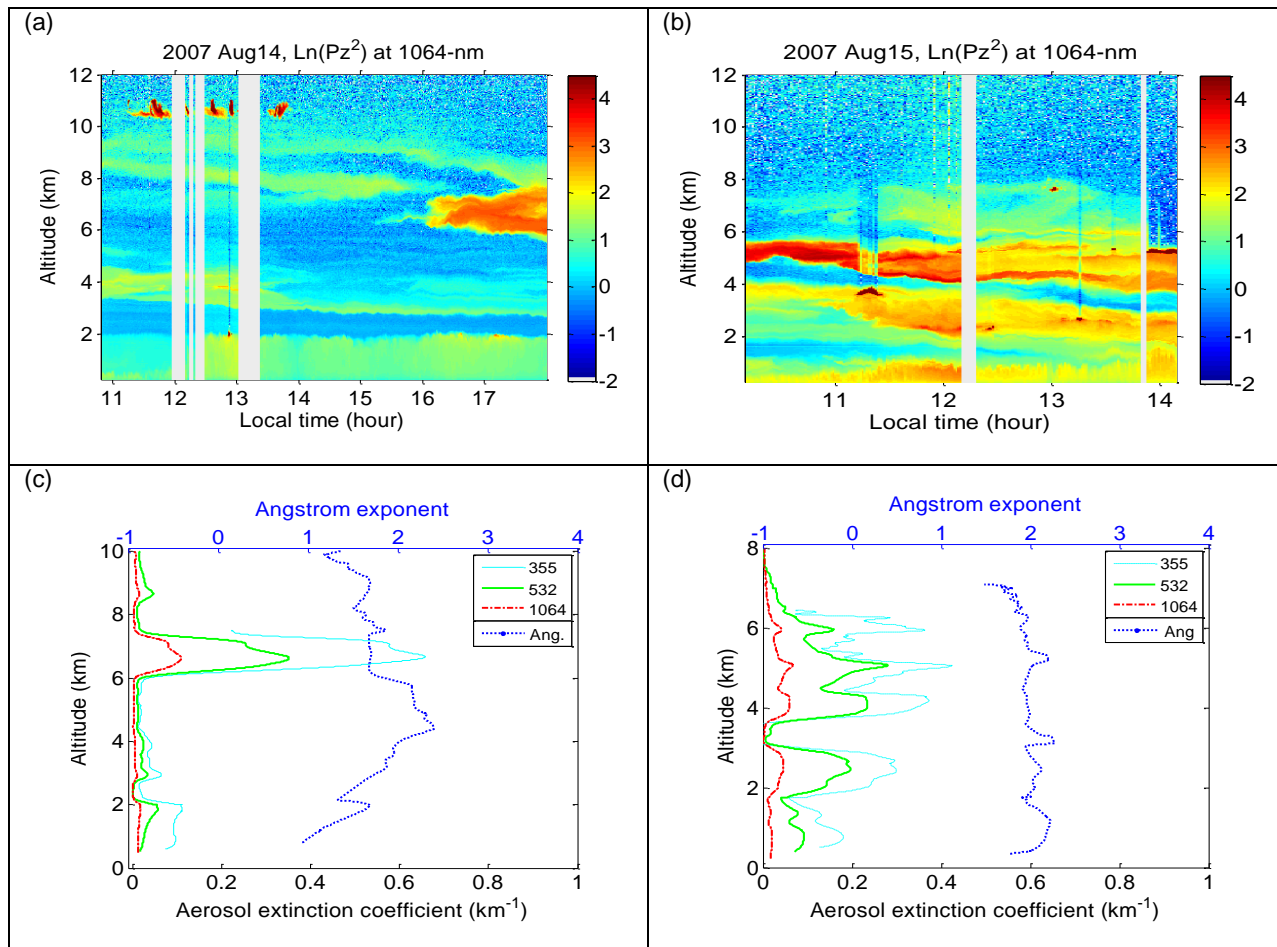
Figure 1 - Time-height cross section of range-corrected lidar returns at 1064-nm on (a) Aug. 14, (b) Aug. 15, 2007; Aerosol extinction and Angstrom exponent profiles at (c)16:30-16:45, Aug.14, (d) 13:35-13:50, Aug.15, 2007.
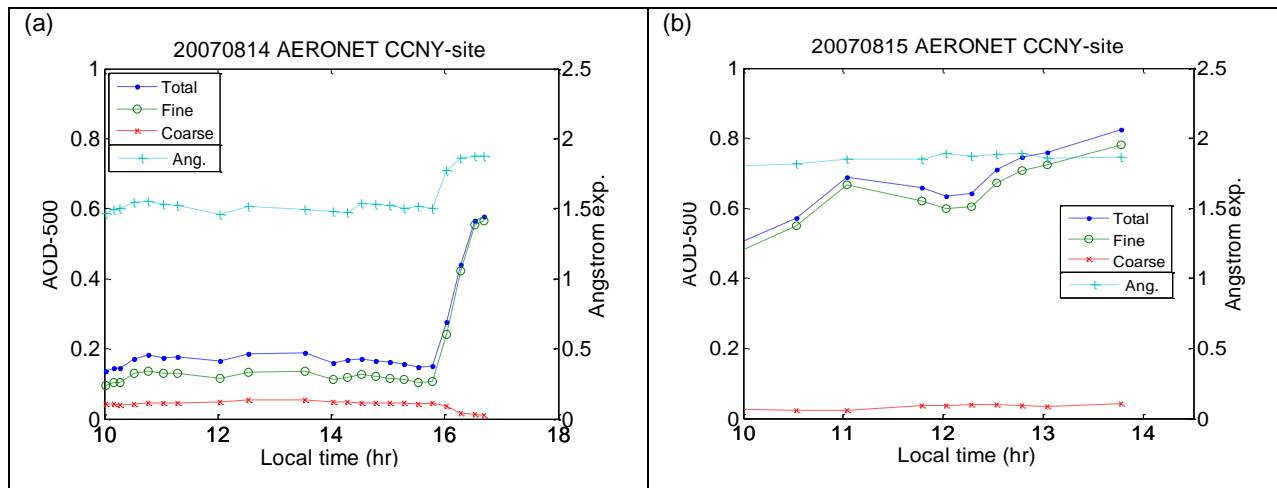
Figure 2 - (a)-(b) Aerosol optical depth and Angstrom exponent observed by AERONET-SP on Aug.14 and Aug.15, 2007.

4.2. Smoke plume sources and transport by satellite observation and model analysis

In particular, dozens of large fires were raging across the Northern Rockies in Idaho and Montana states in mid-Aug 2007. Figure 3 shows the image captured by the Moderate Resolution Imaging

Spectroradiometer (MODIS) on NASA's Aqua satellite at 2:00 p.m. local time (US Mountain Daylight Time) on Aug. 13, 2007. Locations where the sensor detected active fire are outlined in red in US Idaho, Montana and Wyoming states; gray-brown smokes from these fires spread northeasterly and then move easterly across the plains at the foothills of the Northern Rocky Mountains as far away as the US east coast.
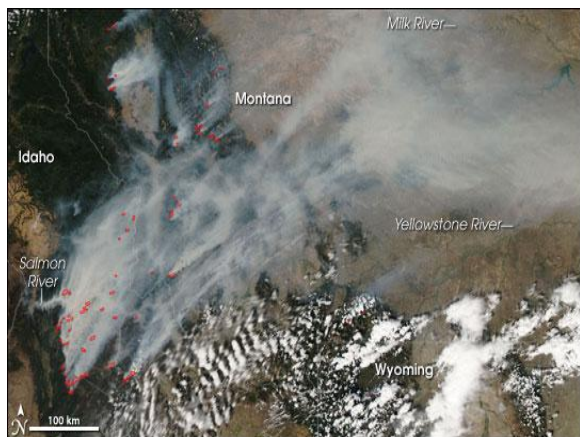
Figure 3 - Images showing smoke and fires area captured by MODIS- Aqua satellite at 2:00 p.m. LT on Aug 13, 2007

Modeled air backward trajectories such as NOAA-HYSPLIT (Hybrid Single Particle Lagrangian Integrated Trajectory) provide a mean to identification of the transport pathway of the air parcels at varying altitudes as specified by lidar observations (Draxler 2003). We plot the 2-day air backward trajectories at 21:00 UTC (17:00 LT) on Aug. 14 at three altitude levels, respectively. Apparently, the air-mass traveled from the Idaho/Montana forest fire area to the lidar site, taking about 40-hour.
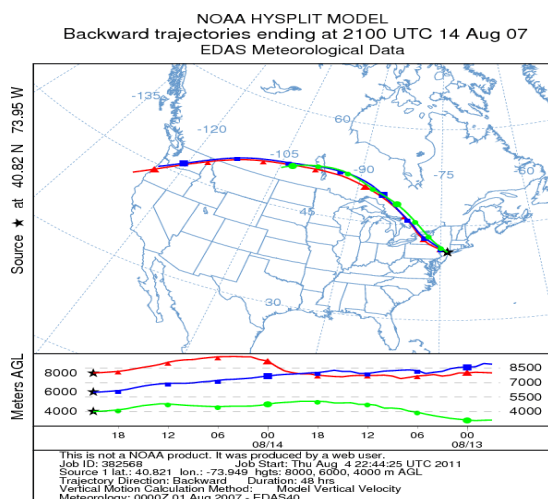
Figure 4 - Two-day backward trajectory analysis by NOAA-HYSPLIT ending at 21:00 UTC (17:00 LT) on August 14 at three altitudes between 4 and 8 km.

The Geostationary Operational Environmental Satellites (GOES) also shows the smoke-plume transport by the air flow in the east direction. GOES Aerosol Optical Depth product illustrates the plume being transported to the northeast coast and arriving to the New York City area by 20:15 UTC (16:15 pm LT).
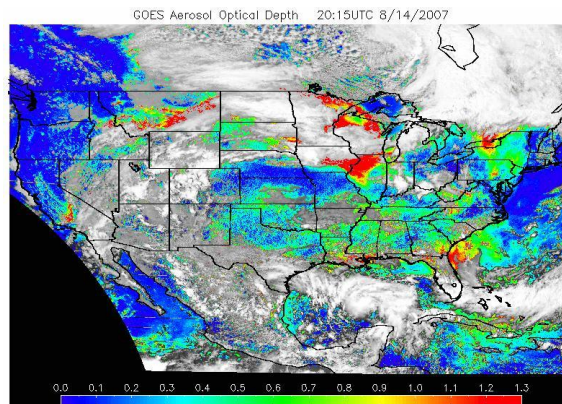
Figure 5 - GOES AOD illustrating the plume transport to the US northeast coast on August 14, 2007 at 12:45 UTC

We explore in more detail the plume observations from satellite platforms. We find that the combined use of MODIS and CALIPSO measurements clearly detail the sources and magnitude of the smoke plumes. Figure 6(a) gives the MODIS/Aqua level-2 aerosol optical depth at 550-nm over the US continent on Aug.15, 2007. The red-pattern with high aerosol optical depths (AOD>=1) indicates the fire-smoke source region in Idaho/Montana. In the US east coast and even over the ocean, the smoke stripes can be seen with the mid-level AOD in magnitude. However, due to cloud cover or sunlit over ocean, MODIS algorithms don't give AOD retrievals over some regions. Also in Figure 6 (a), the lines D1 and D2 are the CALIPSO ground-tracks in the day time while the line N1 is the night track in the US east coast. The orbits D1 and N1 indicate the CALIPSO overpass nearby the CCNY-lidar site while the orbit D2 illustrates the CALIPSO passing near the fire-smoke source. Figure 6(b) gives the total attenuated backscatter coefficients at 532-nm measured by CALIPSO for the night orbit N1 (early morning, ~3 am local time on Aug. 15) in the US east coast. Figure 6(b) clearly shows the dense smoke plume distribution with altitude of 4~6 km over 45º N to 30º N latitudes. For the most time, CALIPSO vertical-feature-mask (VFM) products properly classify the smoke layer as aerosol and further classify them as smoke. However, for some highly dense layers, they are misclassified as clouds, and occasionally some plume layers are misclassified as polluted dust.
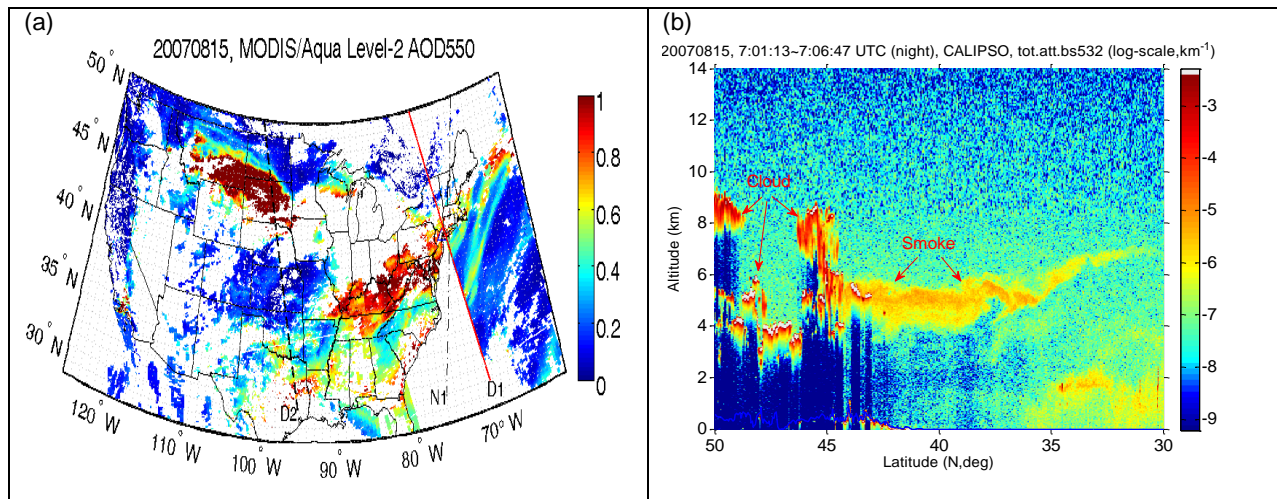
Figure 6 - (a) MODIS/Aqua level-2 aerosol optical depth at 550 nm on 15 August, 2007 (Lines-D1, D2 and N1 are the CALISPO ground-tracks). (b) CALIPSO-attenuated backscatter coefficients at 532-nm at 7:01:12-7:06:47 UTC (track N1, night).

4.3. Smoke influence on local air quality

Figure 7 shows the surface PM$_{2.5}$ loadings on August 13-18 at six-sites in the New York Metropolitan area. On August 14, as expected, the PM$_{2.5}$ loadings were low and in good agreement with lidar measurements of low PBL-AOD. These observations showed no evidence of PBL interaction with free tropospheric plumes, and at the near surface particulate scattering coefficients and concentration remained low, which is a characteristic of clear and relatively unpolluted air above the boundary layer. On the other hand, by the afternoon of August 15, aloft smoke plumes appeared to be mixing down to the surface layer (See Figure 1), likely contributing to significant increase in the surface PM$_{2.5}$ loadings.
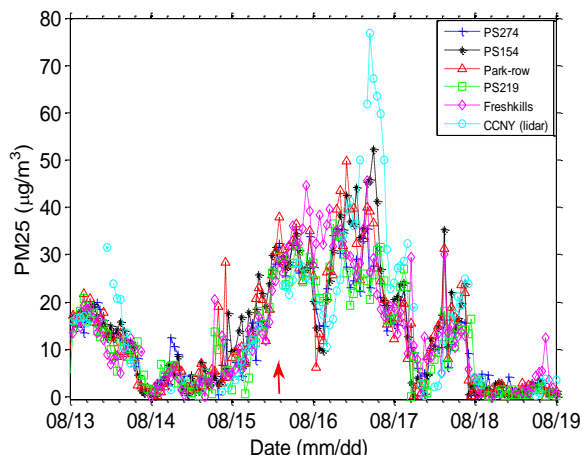
Figure 7 - Ground level PM$_{2.5}$ mass concentration nearby the lidar-site on August 13-19, 2007

5. CONCLUSIONS

We have analyzed the smoke plumes optical properties, long-range transport and their potential influences on the surface air quality with the synergy of ground-based lidar, sunphotometer and satellite observations. The multi-wavelength aerosol extinction profiles are derived from the lidar-sunphotometer combinations, and hence the Angstrom exponent profile is calculated and used to discriminate the smoke plume. The dense aerosol plume layers are located at 2~8 km altitude, and the total AODs reach 0.6-0.8 at 500-nm with large Angstrom exponents (~1.8). The air backward trajectory and satellite observations clearly illustrate the origin and long-distance transport pathway.

Our analysis of the transport of biomass burning smokes to the US east coast from the US northwest demonstrates the importance of accounting for the possibility that intra-continental transported lofted layers can indeed couple mixed into the PBL making tangible contributions to surface air-quality. In particular, the range-resolved lidar observations indicate that the elevated smoke plumes were entrained into the turbulent planetary boundary layer, and the surface PM$_{2.5}$ concentrations show the corresponding increasing trend. These results have important implications for the long-range transport of pollutants and their entrainment to the surface

References

Cattrall, C., J. Reagan, K. Thome, and O. Dubovik, 2005: Variability of aerosol and spectral lidar and backscatter and extinction ratios of key aerosol types derived from selected Aerosol Robotic Network locations, J. Geophys. Res., 110, D10S11, doi:10.1029/2004JD005124.

Colarco, P R., Schoeberl, M R., Doddridge, B G., Marufu, L T., Torres, O., and Welton, E J.: Transport of smoke from Canadian forest fire to the surface near Washington, D.C.: Injection height, entrainment, and optical properties, 2004, J.Geophy.Res., 109, D06203, D06203, doi:10.1029/2003JD004248.

Dubovik, O., Smirnov, A., Holben, B. N., King, M. D., Kaufman, Y. J., Eck, T. F. and Slutsker, I., 2000, Accuracy assessments of aerosol optical properties retrieved from AERONET Sun and sky radiance measurements, J. Geophys. Res., 105, 9791–9806.

Duck, T.J., et al., 2007, Transport of forest fire emissions from Alaska and the Yukon Territory to Nova Scotia during summer 2004, J. Geophys. Res., Vol.112, D10S44, doi:10.1029/2006JD007716.

Duck, T. J., Lucy Crawford, Jonathan Doyle, Steve Beauchamp, and Ray Hoff, 2008, Biomass burning plumes observed with the Dalhousie Raman Lidar, The Canadian Smoke Newsletter, P11~13.

Draxler, R.R., Rolph, G.D., 2003. HYSPLIT (HYbrid Single-Particle Lagrangian Integrated Trajectory) model access via NOAA ARL READY (http://www.arl.noaa.gov/ready/hysplit4.html), NOAA Air Resources Laboratory, Silver Spring, MD

Eck, T. F., B. N. Holben, J. S. Reid, O. Dubovik, A. Smirnov, N. T.O'Neill, 1999, Wavelength dependence of the optical depth of biomass brning, urban, ad desert dust aerosols, J.Geophys. Res., 104, 31,333–31,349.

Fernald, F. G., 1984, Analysis of atmospheric lidar observations: some comments, Appl. Opt. 23, 652-653.

Guan, H., R. Esswein, J. Lopez, R. Bergstrom, A. Warnock, M. Follette-Cook, M. Fromm, and L.T. Iraci, 2010, A multi-decadal history of biomass burning plume heights identified using aerosol index measurements, Atmos. Chem. Phys., 10, 6461-6469.

Holben, B.N., T.F.Eck, I.Slutsker, D.Tanre, J.P.Buis, A.Setzer, E.Vermote, J.A.Reagan, Y.Kaufman, T.Nakajima, F.Lavenu, I.Jankowiak, and A.Smirnov, 1998, AERONET - A federated instrument network and data archive for aerosol characterization, Rem. Sens. Environ., 66, 1-16.

Klett, J. D., 1981, Stable analytical inversion solution for processing lidar returns, Appl. Opt. 20(2), 211-220.

Kaufman, Y. J., D. Tanré, L. Remer, E. Vermote, A. Chu, and B. N. Holben, 1997, Remote sensing of tropospheric aerosol from EOS-MODIS over the land using dark targets and dynamic aerosol models, J. Geophys. Res., 102, 17051-17067.

Kaufman, Y. J., I. Koren, L. A. Remer, D. Rosenfeld and Y. Rudich, 2005, The effect of smoke, dust, and pollution aerosol on shallow cloud development over the Atlantic Ocean, *Proc. Nat. Acad. Sci.*, 102, 11207-11212.

Landulfo, E., A. Papayannis, P. Artaxo, A. Castanho, A. Z. de Freitas, R. F. Souza, N. D. Vieira Junior, and D. S. Moreira, 2003, Synergetic measurements of aerosols over São Paulo, Brazil using LIDAR, sunphotometer and satellite data during the dry season, Atmos. Chem. Phys., 3, 1523-1539, doi:10.5194/acp-3-1523-2003.

Martin, M., J.A. Logan, D. Kahn., F.Y. Leung, D. Nelson, D. Diner, Smoke injection heights from fires in North America: analysis of 5 years of satellite observations, Atmos. Chem. Phys. Discuss., 9, 20515-20566, doi:10.5194/acpd-9-20515-2009, 2009

Münkel, C., J. Räsänen, 2004, New optical concept for commercial lidar ceilometers scanning the boundary layer, Proc. SPIE 5571, pp. 364-374, doi:10.1117/12.565540

Omar, A. H., J-G. Won, D. M. Winker, S-C. Yoon, O. Dubovik, and M. P. McCormick, 2005, Development of global aerosol models using cluster analysis of Aerosol Robotic Network (AERONET) measurements, *J. Geophys. Res.*, 110, D10S14, doi:10.1029/2004JD004874.

O'Neill, N. T., T. F. Eck, A. Smirnov, B. N. Holben, and S. Thulasiraman, Spectral Discrimination of Coarse and Fine Mode Optical Depth, J. Geophys. Res., 108(D17), 4559, doi:10.1029/2002JD002975, 2003.

O'Neill, N. T., T.F. Eck, B.N. Holben, A. Smirnov, A. Royer, Z. Li, (2002). Optical properties of Boreal Forest Fire Smoke Derived from Sun photometry, Journal of Geophysical Research, 107, D 11, 10.1029/2001JD000877.

Pelon, J., C. Flamant, P. Chazette, J.-F. Leon, D. Tanre, M. Sicard, and S. K. Satheesh, 2002, Characterization of aerosol spatial distribution and optical properties over the Indian Ocean from airborne LIDAR and radiometry during INDOEX'99, *J. Geophys. Res.*, 107(D19), 8029, doi:10.1029/2001JD000402.

Sassen, K., and V. I. Khvorostyanov, 2008, Indirect cloud effects from boreal forest fire smoke: Evidence for ice nucleation from polarization lidar data and cloud model simulations. Environ. Res. Lett., 3(2): doi:10.1088/1748-9326/3/2/025006.

Wu, Y., S. Chaw, B. Gross, F. Moshary, and S. Ahmed, 2009, Low and optically thin cloud measurements using a Raman-Mie lidar, Appl. Opt. 48, 1218-1227.